

## Final Report

### LIPS and Bones: Application of LASER-based geological techniques to bone content research

Principal Investigator  
Dr. Harjit Pal Bhattoa

30<sup>th</sup> of November, 2015

## TABLE OF CONTENT

1. Introduction	2
2. Aims of the Project	3
3. Methods and Materials	3
Sample preparation	3
Analytical techniques	4
Samples	5
4. Results	5
Mathematical modelling of the inorganic compartment of the bone tissue	10
LIPS analyses in segmented networks	11
LIPS analyses in regular networks	12
Comparison of qCT attenuation coefficient with the geological “ $\rho$ ”	15
MEDI-LIPS instrument: summarized description	16
The “LIPS” processing software: instrument control and data analysis	18
Calibration of the MEDI-LIPS instrument	19
5. Conclusion	24
6. Alterations from the original research plan	24
7. Finance and Publications	25
8. References	26

## Introduction

The assessment of bone structure and bone content may be essential in various bone and calcium homeostasis disorders. Bone densitometry (DEXA) has been widely used to determine bone density in osteoporosis (OP) and other conditions [1]. Bone structure may be assessed by micro-CT or high resolution MRI techniques [1,2]. Yet, the assessment of bone mineral content and the concentration of various elements in the bone have not yet been elucidated. For such analyses, bone biopsy may be needed. This is rather painful, and not all individuals may be biopsied [1]. It is evident that bone biopsy will never become a routinely used diagnostic test [1,2]. These limitations also hinder the conduction of various clinical studies using anti-osteoporotic drugs. It is feasible to study the effects of such agents on bone density and on the outcome of fractures, however, mostly invasive techniques are needed in order to further dissect the cellular and metabolic effects of drugs.

These issues lead to the idea to apply geological techniques to bone research. Indeed, inorganic minerals are the most abundant constituents of bones. Furthermore, as described later, there have been few initial attempts using geological, mostly LASER-based methods to assess the chemical composition of bones.

The determination of the concentration of various minerals and their structure, major- and trace element content in the bone may have significant relevance in and beyond the field of medicine. The amount of various elements may differ between healthy and unhealthy bone. Furthermore, certain trace elements, such as strontium (Sr) used in the treatment of osteoporosis, lithium (Li) used to treat psychiatric and thyroid diseases, and aluminum (Al) and lanthanum (La) in hemodialyzed patients may accumulate in the bone. The determination of these elements could be used in toxicology studies. Forensic medicine may use such techniques in order to assess the accumulation of lead (Pb) or arsenic (As) in various tissues [3-8]. Additionally, LASER techniques have also been used to assess bone age in archeology [9]. Nonetheless, till date very few studies, mostly carried out on animals using ICP-MS (inductively coupled plasma spectrometry) have been published [3-5,8,10].

A number of elements may play a role in bone physiology and pathology. Al, Cd, Mo, Pb, Zn, Cu, Li, Mg, Mn, Fe, Sr and their salts have been implicated in bone mineralization, osteoblast and osteoclast function, bone stiffness and elasticity and numerous aspects of bone pathology. Al deposition concurrent to hemodialysis or the excessive use of antacids may inhibit bone mineralization and may lead to osteodystrophy or osteomalacia [11]. The phosphate-binding La, also used in nephrology, is a functional mimetic of calcium (Ca). It may accumulate in bone and may exert both physiological and pathological effects [12,13]. Cd is an antagonist of Ca and vitamin D absorption, its excess may lead to osteoporosis and osteomalacia with fractures or kidney stones [14]. Mo toxicity leads to impaired bone development and neurodegeneration [15]. Acute Pb toxicity can be determined from blood, but cumulative intoxication may be assessed in bone [16]. Pb inhibits fracture healing [17]. Zn and Cu have important physiological relevance for bone. Zn and Cu deficiency may lead to impaired bone matrix synthesis and osteoporosis [18,19]. Li carbonate has been used to treat depression and thyroid disorders. Li toxicity may lead to hyperparathyroidism and bone loss [20,21]. Mg is crucial for bone formation and homeostasis [22]. Mg deficiency may lead to increased resorption, impaired elasticity and bone loss [22]. Mn is a natural constituent of bone. Mn toxicity may be observed among miners and factory workers. Assessment of Mn in serum samples is not informative. There have been attempts using a neutron-activation assay to assess Mn content in bones of the hands [23]. Excess of Fe often leads to bone loss. Fe may inhibit osteoblast and stimulate osteoclast function [24]. With the introduction of Sr ranelate, an anti-osteoporosis agent, the determination of Sr in the bone may be necessary [25,26].

Thus, bone research and geology may complement each other and this may open a new perspective for the development and application of new LASER-based geological techniques to study the chemical composition of bones.

Laser ablation inductively coupled plasma mass spectrometry (LA-ICP-MS) and laser induced plasma spectrometry (LIPS) has long been used in the Geological Institute of Hungary (MÁFI), currently known as the Geological and Geophysical Institute of Hungary (MFGI). In LIPS, a high power density (109-1012 Watt/cm<sup>2</sup>) laser beam is focused on a small sized target surface (10-100 µm in diameter). The generated vapor enters the laser-induced plasma above the target where its excitation takes place. By resolving the emitted radiation, a spectrum is observed for the determination of elemental composition. In the LA-ICP-MS the mixture of vapor and fragmented particles are cooled down by Ar carrier gas for transporting into the ICP source for spectroscopic observation by optical emission spectrometry (OES) or mass spectrometry (MS)

[27,28]. The construction of portable LIPS systems is a hot research topic. Primarily space research [29] and military applications [30] have been published, however, geological applications [31] are also important. The ImaGeo-LIPS system was developed at the MÁFI in the late 1990's [32,33]. The ImaGeo Corescanner has been used in many geological studies for measuring the spatial distribution of structures and geological phenomena in drillcores at various sites of Hungary as well as in international collaborations [34-38]. Several studies have been executed with the LIPS module attached to the corescanner, as a field instrument; to determine the chemical composition of drillcore rocks [39,40] and later on additional modifications have also been facilitated [38,40,41-43]. Recent collaborative work between the University of Debrecen and MFGI has conceived a vision to apply the LIPS technique to bone research.

The research group at the University of Debrecen has performed several human studies on primary and secondary osteoporosis [44-51]. Additionally, have applied a methodology of local delivery of calcium and phosphate into animal bones [44,45], which may also have applications for the LIPS technique.

## **Aims of the Project**

1. To test the LIPS instrument and incorporated software on healthy and pathological human bones
2. To perform detailed elemental composition analysis of normal, osteoporotic and malignant bone samples in order to standardize in vitro evaluation.
3. To confirm LIPS results by ICP-MS and other standardized laboratory analytical methods.
4. To develop a new instrument suitable for in vivo human assessments and to develop a protocol that is not painful and ethically acceptable.
5. To assess other applications in medicine, such as drug accumulation and toxicology.

## **Material and Methods**

We think, however, that before the application of the LIPS technique to human bones a robust baseline study is necessary to characterize fully the chemical and mineralogical/organic composition of bones. To achieve this a very wide range of (mainly geological reference) analytical tools, i.e., X-ray diffraction (XRD), thermogravimetry (TG), Fourier transform infrared spectrometry with attenuated total reflectance accessory (FTIR-ATR), inductively coupled mass spectrometry (ICP-MS) and inductively coupled optical emission spectrometry (ICP-OES) were applied to measure organic and inorganic composition of 5 bovine bone samples. This dataset, on one hand, would make it possible to use this independently determined chemical composition to calibrate the LIPS instrument. On the other hand, the mineralogical and organic composition of bones could contribute to better understand possible matrix effect during LIPS analysis.

Peripheral qCT was done on all samples before any of the above procedures was done. The Hungarian Science and Research Ethics Committee (ETT-TUKEB) approved the study protocol.

## **Sample preparation**

During the pre-analytical phase, the organic matter (meat and marrow) was removed from the bones first mechanically and then by boiling in water with 1% hydrogen peroxide. The bones were cut into smaller pieces using a saw, and then ground further to achieve particle sizes between 2 and 63  $\mu\text{m}$  and get roughly around 10-20 grams for further analysis.

For the X-ray diffraction (XRD; 1 gram), thermogravimetry (TG; 100 mg) and attenuated total reflectance Fourier transform infrared spectroscopy (ATR-FTIR; ~30 mg) this powdered bone was used, in the respective quantities mentioned, to determine their organic and inorganic compounds.

For the chemical analysis, the powder (~ 3 grams) was chemically exposed, as a result of which the powder was dissolved with „aqua regia” facilitated by microwaves and a clear homogenous solution was obtained. This solution was used to determine the major and trace elements composition using the inductively coupled plasma optical emission spectrometry (ICP-OES) and inductively coupled plasma mass spectrometry (ICP-MS) techniques.

All analytical measurements above were all implemented at the Geological and Geophysical Institute of Hungary.

## **Analytical techniques**

### ICP-OES

Analyses were undertaken on a Jobin Yvon ULTIMA 2C inductively coupled plasma-optical emission spectrometer, equipped with both monochromator and polychromator. For calibration, the GBW07109–GBW07114 rock standards (certified reference rock samples of the Institute of Rock and Mineral Analysis, Ministry of Geology and Mineral Resources, China) were applied.

### ICP-MS

ICP-MS analyses were done using a VG PlasmaQuad II STE equipment with the same standards as for the ICP-OES analysis.

### XRD

For the X-ray powder diffraction analysis by Phillips PW 1730 diffractometer (Cu cathode, 40 kV and 30 mA tube-current, graphite monochromator, goniometer speed 2°/minute), powdered bone samples were used. A semi-quantitative assessment of the relative concentrations of phases was performed by relative intensity ratios and full width at half maximum (FWHM) of specific reflections of minerals by using XDB Powder Diffraction Phase Analytical software 2.7 (Sajó, 1994).

### TG

Thermal analysis were carried out by Derivatograph-PC from room temperature (20 °C) to 1000°C (10°C/minute) using Al<sub>2</sub>O<sub>3</sub> as inert material. 100 mg of samples was heated in ceramic crucible. The quantitative determination of the thermally active minerals is based on stoichiometric calculations of decomposition processes of the identified minerals due to loss of mass during heating (Paulik and Paulik, 1981; Földvári, 2011). Loss of molecular water was also measured.

### FTIR

Powdered bone samples were investigated by a Fourier-transform infrared spectrometer (Bruker Vertex 70) coupled to a single pass ATR cell (Platinum ATR) in the mid-infrared spectral region (400–4000 cm<sup>-1</sup>). For the analysis a liquid nitrogen cooled MCT detector was used. All samples were placed in roughly equal amount (~30 mg) in polished glass containers and heated for at least 30 min at 80°C directly before the measurements. Glass containers were closed with properly sealing grinded glass lids and wrapped in parafilm immediately after heating. This procedure is believed to remove the majority of the absorbed water that could modify absorption characteristics.

For samples and their respective backgrounds, 64 scans were acquired at a nominal resolution of 4 cm<sup>-1</sup>. The sample powder is pressed with constant pressure on a small diamond crystal plate which allows obtaining reproducible spectra from different sample batches.

Baseline and extended ATR corrections were done by applying OPUS 6.5 software package for processing the spectra before evaluation. For the advanced ATR correction 1 reflection, 45° of incidence angle and 1,54 refractive index were assumed.

## Samples

A total of 5 male bovine tibial bone samples from the same animal were used for the initial examinations (samples: Bull\_1, Bull\_2, Bull\_3, Bull\_4, Bull\_5).

As a subsequent research step, it was proposed that 15 female bovine bone samples of different ages be studied to deduce the age related changes with the reference geological method. Furthermore, in order to investigate the similarity between bone and tooth, 3 teeth samples belonging to the studied bovine cohort, were also proposed to be studied by the reference techniques.

Additionally, 15 human cadaver tibial bone samples of various ages were also proposed to be studied by the reference techniques. This was to study the reproducibility of the techniques mentioned above in the human bone samples.

## Results

As an initial step, the peripheral qCT examination of the 5 male and 15 female bovine tibia bone samples, 3 molar teeth and 15 human cadaver tibia bone samples was carried out in the University of Debrecen. These samples were forwarded to the Geological and Geophysical Institute of Hungary in Budapest for analyses with the 5 reference geological techniques.

Bulk major and trace element composition of bones determined by inductively coupled plasma optical emission spectrometry (ICP-OES) and inductively coupled plasma mass spectrometry (ICP-MS) analysis results from solution of the 5 male bovine bone samples is presented in table 1 and 2.

Table 1. Bulk major element composition of bones determined by inductively coupled plasma optical emission spectrometry (ICP-OES) analysis from solution (given in ppm wt.% but for elements with italics in wt.%).

Elements	Sample identity				
	Bull_1	Bull_2	Bull_3	Bull_4	Bull_5
Al <sub>2</sub> O <sub>3</sub>	178	163	235	269	285
BaO	61.6	61.7	61.7	74.0	60.3
Fe <sub>2</sub> O <sub>3</sub>	521	425	438	1245	397
K <sub>2</sub> O	385	114	448	566	462
<i>MgO</i>	<i>0.655</i>	<i>0.654</i>	<i>0.682</i>	<i>0.715</i>	<i>0.658</i>
MnO	7.57	10.3	4.33	9.07	6.29
<i>Na<sub>2</sub>O</i>	<i>0.781</i>	<i>0.621</i>	<i>0.753</i>	<i>0.736</i>	<i>0.773</i>
SiO <sub>2</sub>	560	274	609	678	661
<i>SO<sub>3</sub></i>	<i>0.174</i>	<i>0.361</i>	<i>0.186</i>	<i>0.202</i>	<i>0.176</i>
SrO	304	268	296	293	293
TiO <sub>2</sub>	6.60	38.9	7.04	11.9	7.79
<i>CaO</i>	<i>35.00</i>	<i>33.26</i>	<i>34.67</i>	<i>34.52</i>	<i>35.03</i>
<i>P<sub>2</sub>O<sub>5</sub></i>	<i>28.07</i>	<i>26.81</i>	<i>28.35</i>	<i>28.43</i>	<i>28.87</i>
Total	64.9	61.8	64.9	64.9	65.7

Table 2. Bulk trace element composition of bones determined by inductively coupled plasma mass spectrometry (ICP-MS) analysis from solution (given in ppm wt.%).

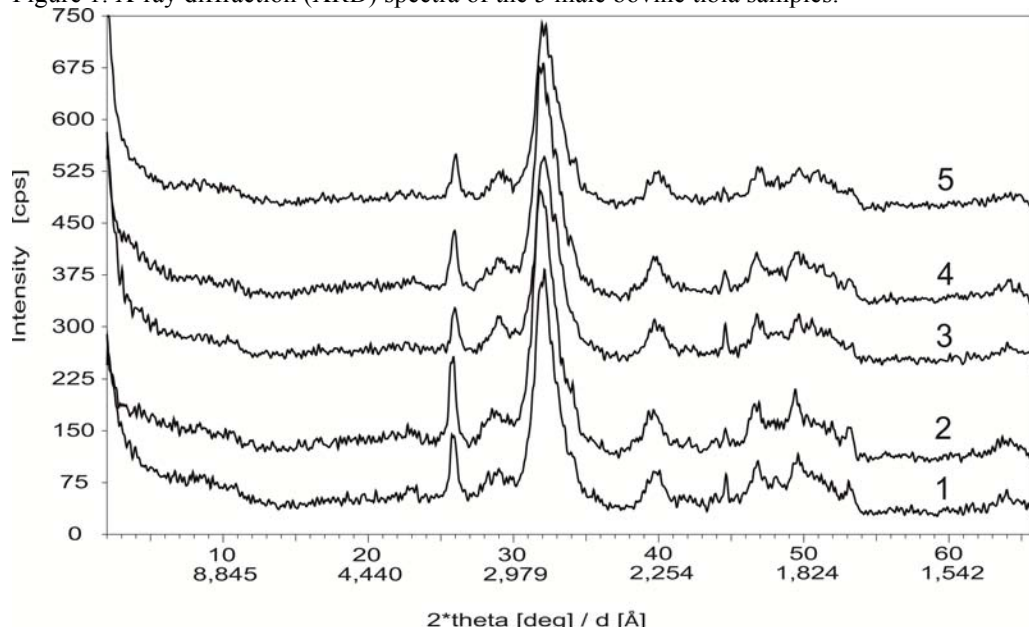
Elements	Sample identity				
	Bull_1	Bull_2	Bull_3	Bull_4	Bull_5
Cr	44.2	56.6	41.0	65.2	38.1
Mn	6.56	9.21	3.95	8.28	6.23
Co	0.85	0.39	0.36	0.52	0.82
Ni	21.6	5.74	2.42	4.98	19.9
Cu	11.2	4.14	5.80	10.4	11.7
Zn	67.4	103	63.2	82.1	79.3
Rb	0.31	0.15	0.34	0.42	0.44
Sr	291	249	283	277	287
Y	0.08	0.06	0.06	0.16	0.07
Mo	1.56	0.83	0.53	1.01	1.28
Cd	<0.02	0.03	<0.02	<0.02	<0.02
Sn	143	2.74	13.5	11.7	12.3
Sb	1.91	0.53	0.53	0.39	1.13
Cs	<0.05	<0.05	<0.05	<0.05	<0.05
Ba	69.2	66.9	68.2	80.3	69.7
La	0.15	0.07	0.13	0.18	0.26
Ce	0.20	0.16	0.22	0.31	0.21
Pr	<0.05	<0.05	<0.05	<0.05	<0.05
Nd	0.92	0.13	0.61	1.43	0.60
Tl	<0.02	<0.02	<0.02	<0.02	<0.02
Pb	77.6	<0.05	4.51	3.86	5.87
Bi	0.10	<0.05	<0.05	<0.05	0.07
Th	<0.05	<0.05	<0.05	<0.05	<0.05
U	<0.05	<0.05	<0.05	<0.05	<0.05

As per the results of the chemical analyses, it was found that the bones are, in principle, homogenous. Among the trace elements, it was As that could not be measured with certainty, and Li could only be measured by using ICP-OES. Some contamination from the utensils used during the sample preparations could not be ruled out while evaluating the Fe, Al, Ni, Sn and Pb concentrations. These elements were determined in higher concentrations in the sample that was analyzed first in the series, suggesting that the origin of this contamination may be the metal tools used during the sample preparation.

Since the total for the chemical measurements accounted only for ~ 65 wt.%, it may well be assumed that apart from the inorganic/mineral components, the “missing” weight consists of the organic part of the bones (e.g., C, H, S, N, O). These organic components of the bone cannot be constrained by the applied sample preparation and ICP techniques.

Among the mineral components of the bone, the X-ray analysis could only detect apatite (Figure 1). The exact type of the apatite (OH, F or Cl dominance among the anions), however, could not be unambiguously constrained. The relatively narrow reflections characteristic for apatite implied that the apatite was better crystallized, which suggested that the bones belonged to an aged animal. This is because the bands with decreasing half widths refer to higher crystallinity of apatite crystals, which improves with ageing of bones [52]. The half width of the band at ~ 26° is particularly sensitive to crystalline ordering of apatite [53].

Figure 1. X-ray diffraction (XRD) spectra of the 5 male bovine tibia samples.



Due to the relatively low total inorganic/mineral content of the bones and the fact that the XRD could only detect apatite as a mineral component, it seemed justified to carry out complementary TG and FTIR-ATR measurements to determine the remaining inorganic/mineral and organic phases of the bones.

During the TG examination, which determines the weight loss as a function of increasing temperature, the colour of the bone samples changed from light grey to whitish-yellow. The weight loss of the bone samples can be differentiated into 4 distinct phases. In the first phase ( $\sim 45^{\circ}$ - $205^{\circ}$  C), the water (i.e. partly bound to the organic material) is lost. In the second phase ( $\sim 200^{\circ}$ - $400^{\circ}$  C), the organic matter is burnt out during an exothermic reaction. In the third phase ( $\sim 400^{\circ}$ - $650^{\circ}$  C), the remaining organic material and the  $\text{OH}^-$  content is lost. In the fourth phase (above  $650^{\circ}$  C), along with a small decrease in weight, most probably the carbonates are decomposed. An attempt was made to determine the composition of carbonated hydroxyapatite from the amount of  $\text{CO}_3$  lost, however, this was complicated by the presence of poorly crystallized carbonates (i.e. calcite, dolomite) that could also contribute to the released  $\text{CO}_2$  content [54].

The exothermic band ( $732^{\circ}$  –  $799^{\circ}$ C) suggests a phase transition from apatite to  $\beta$ -tricalcium phosphate. Furthermore, it needs to be mentioned that the exothermic reaction does not happen in the bone samples treated with additional hydrogen peroxide.

The total volatile content of the samples was about 35 wt.%. This together with the 65 wt.% total of the chemical analysis (i.e., inorganic components) yields a total approaching very closely 100 wt.%. Since a large portion of the volatile content ( $\text{H}_2\text{O}$ ,  $\text{CO}_2$ , etc.) is liberated from the organic components, it can be concluded that the inorganic/mineral to organic ratio of the examined bone samples is  $\sim 35:65$ . Furthermore, a small amount of carbonate may originate either from the apatite or the carbonate minerals, such as calcite or dolomite. This means that besides apatite, carbonate may also be present as an inorganic mineral constituent. Nonetheless, carbonates cannot be detected by XRD most probably due to their poor crystallinity. The presence of calcite and/or dolomite is also supported by the considerable amount of Mg ( $\sim 0.6$  wt.%) observed in the chemical compositions. This is because Mg is not a major constituent of neither the apatite or the organic portion of the bone.

The chemical composition also suggests the presence of salts, as the sodium content of the bone samples is relative high (0.7 wt.%). Sodium –similar to Mg - is not a major component of apatite, carbonate or the organic portion. The TG analysis of the bone samples has revealed that we can identify the missing 35 wt.% mass as organic matter besides apatite and carbonate. However, the TG analysis does not get us closer to the composition of the organic matter in the bone samples. Quantitative results of termogravimetric analysis of bones are presented in Table 3.

Table 3. Quantitative results of thermogravimetric analysis of bones (weight is given in wt.%).

Sample identity	water	organic material	volatile content above 400 °C	total volatile content	CO <sub>2</sub>	apatite*	exotherm band**
Bull_1	6.44	14.7	13.5	34.6	2.39	52.6	733
Bull_2	6.71	15.2	15.1	37.0	3.69	81.3	777
Bull_3	6.93	13.7	19.9	40.6	3.40	74.9	799
Bull_4	6.48	14.5	14.2	35.3	3.16	69.6	755
Bull_5	6.56	13.1	12.6	32.3	3.21	70.7	772
Bull_1 treated with H <sub>2</sub> O <sub>2</sub>	6.15	4.41	3.5	14.1	1.88	41.4	—

\* calculated apatite content from carbonate content

(<http://webmineral.com/data/Carbonate-hydroxylapatite.shtml>)

\*\* exotherm band referring to phase transition

Thus, samples were investigated further by Fourier-transform infrared spectrometer (Bruker Vertex 70) coupled to a single pass ATR cell (Platinum ATR) in the mid-infrared spectral region (400-4000 cm<sup>-1</sup>). For the analysis a liquid nitrogen cooled MCT detector was used. It should be noted that each spectrum displays spectral features of the diamond ATR crystal between ~1800 and 2200 cm<sup>-1</sup>. All samples were placed in roughly equal amount (3-5 mg) in polished glass containers and heated for at least 30 min at 80°C directly before the measurements. Glass containers were closed with properly sealing grinded glass lids and wrapped in parafilm immediately after heating. This procedure is believed to remove the majority of the absorbed water that could modify absorption characteristic and may prevent aggregation of mineral particles [55].

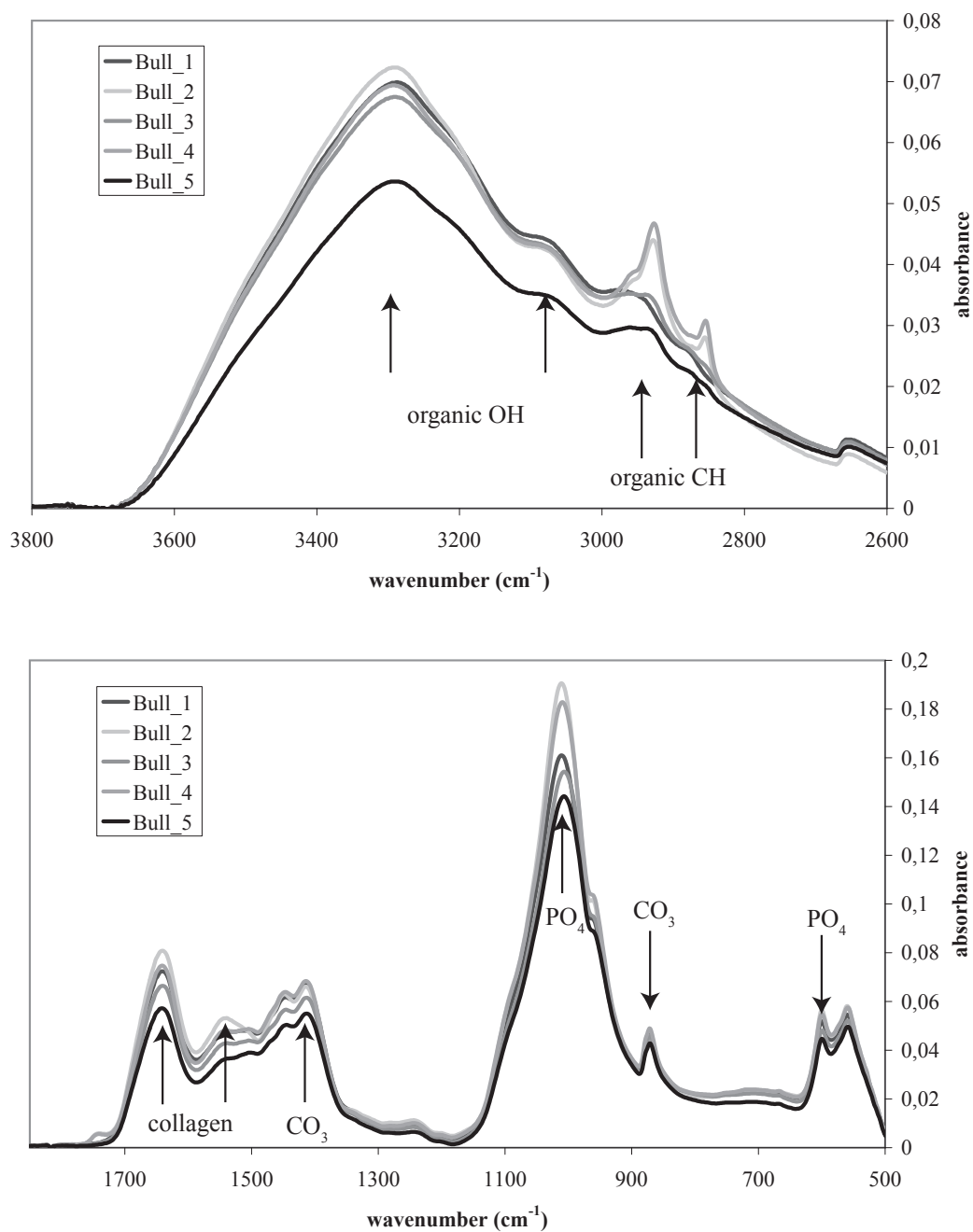
For samples and their respective backgrounds, 128 scans were acquired at a nominal resolution of 4 cm<sup>-1</sup>. The sample powder is pressed with constant pressure on a small diamond crystal plate, which allows obtaining reproducible spectra from different sample batches.

Baseline and extended ATR corrections were done by applying OPUS 6.5 software package for processing the spectra before evaluation. For the advanced ATR correction 1 reflection, 45° of incidence angle and an average 1.54 refractive index were assumed. Even if this later refractive index is an arbitrary choice and may introduce some uncertainty, this value seems to be an optimal choice for most of the minerals occurring in the studied samples.

The FTIR-ATR analysis revealed that the organic portion consists of collagens containing amide groups, since their typical bands (OH, CH, CO, NC) can be clearly identified in the infrared spectra [53,56-58]. Furthermore, the area under the amide bands correlates well with the organic content determined by TG. It can also be observed that with the increasing content of the organic portion, the concentration of S also increases.

The infrared spectra also illustrate that the apatite either does not or contains only minute quantities of hydroxyl, furthermore, there may be some carbonate substitution for phosphate. As per the spectra, the carbonates may be present in the form of carbonate crystals (MgCO<sub>3</sub>) as well (figure 2). In a recent breakthrough study in American Mineralogist it was demonstrated that H<sub>2</sub>O and CO<sub>2</sub> incorporation even into strongly hydroxyl deficient apatites can play a key role in influencing its physical and medical properties [59].

Figure 2. Attenuated total reflectance Fourier transformed infrared (FTIR-ATR) spectra of the 5 male bovine tibia samples. Assignment of main bands is based on reference numbers 53 and 57.



## Mathematical modelling of the inorganic compartment of the bone tissue.

The structural similarities between the inorganic component of bone tissue and geological formations make it likely that mathematical models may be used to determine weight percentage composition of the different mineral element oxides constituting the inorganic component of bone tissue. The determined weight percentage composition can be verified with the determination of element oxide concentration values by laser induced plasma spectroscopy and inductively coupled plasma optical emission spectrometry. It can be concluded from calculated weight percentage composition of the inorganic component of bone tissue and laboratory analyses that the properties of bone tissue are determined primarily by hydroxyl apatite.

The formulae of the mineral constituents in the inorganic component and the composition of the elementary oxides for mathematical modelling is presented below:

Inorganic compartment		Chemical equaiton	Oxide composition
1.	Hydroxyl apatite	$\text{Ca}_{10}(\text{PO}_4)_6(\text{OH})_2$	<b>10 CaO + 3 P<sub>2</sub>O<sub>5</sub> + H<sub>2</sub>O</b>
2.	Calcite	$\text{Ca}(\text{CO}_3)$	<b>1 CaO + 1 CO<sub>2</sub></b>
3	Magnesite	$\text{Mg}(\text{CO}_3)$	<b>1 MgO + 1 CO<sub>2</sub></b>
4	silicium-dioxide	$\text{SiO}_2$	<b>1 Si + 2 O<sub>2</sub></b>
5	alkalic salts	NaCl és KCl	<b>1Na + 1Cl és 1K + 1Cl</b>

The below mentioned relationship (equation) can be utilized to calculate the elementary oxide weight percentage composition of the mineral constituents in the inorganic component:

$$[\text{mass percentage}] * [\text{molecular weight}] * [\text{molecular number}] = [\text{corrected molecular weight}]$$

$$[\text{MP}] * [\text{MW}] * [\text{MN}] = [\text{CMW}]$$

The elementary oxide concentration values can be presented as weight percentage when the corrected molecular weight of each mineral component are known:

$$[\text{Oxide weight precentage}] = [\text{corrected molecular weight}] * [\text{density}_{\text{mineral}}] /$$

$$[\text{molecular weight}_{\text{mineral}}] / [\text{density}_{\text{bone tissue}}]$$

$$C_{\text{oxide}} = [\text{CMW}] * [\rho_{\text{mineral}}] / ([\text{MW}_{\text{mineral}}] / [\rho_{\text{bone tissue}}])$$

where:

$C_{\text{oxide}}$	elementary oxide weight percentage
MP	mass percentage
MW	molecular weight of the individual oxides
MN	molecular number
CMW	corrected molecular weight
$\rho_{\text{mineral}}$	density of the mineral constituents in the inorganic component
$\rho_{\text{bone tissue}}$	bone tissue density (laboratory measurement)
$\text{MW}_{\text{mineral}}$	molecular weight of the mineral constituents in the inorganic component

An example of the mathematical modelling of the bone tissues' mineral constituents in the inorganic component is shown in table 4. The elementary oxide weight percentage ( $C_{\text{oxide}}$ ) can be computed with the corrected molecular weight (CMW), the mineral constituents' molecular weight ( $\text{MW}_{\text{mineral}}$ ) and density ( $\rho_{\text{mineral}}$ ) and the bone tissue density ( $\rho_{\text{bone tissue}}$ ). The bone tissue density can be derived by laboratory measurement or can be a calculated value.

Table 4. The mathematical modelling of the bone tissues' mineral constituents in the inorganic component.

Minerals constituting the inorganic part		Mass %	Mineral density	density %	Chemical equation	Mol. weight	Mol. number	Mol.wt.* Mol. no.	Corrected mol. wt.	weight %
		(MP)	$\rho_{\text{mineral}}$	(MP)* $\rho$		(MW)	(MN)	(MW)*(MN)	(CMW)	$C_{\text{oxide}}$
1	Calcite	0.0200	2.700	0.054	CaO CO <sub>2</sub>	56.080 44.000	1 1	56.080 44.000	1.122 0.880	1.57 1.23
2	Hydroxyl apatite	0.3500	3.100	1.085	CaO P <sub>2</sub> O <sub>5</sub> H <sub>2</sub> O	56.080 141.96 18.000	10 3 1	560.800 425.868 18.000	196.28 149.05 6.30	31.40 23.85 1.01
3	Magnesite	0.0100	3.000	0.030	MgO CO <sub>2</sub>	40.320 44.000	1 1	40.320 44.000	0.40 0.44	0.74 0.81
4	Silicium-dioxide	0.0050	2.650	0.013	SiO <sub>2</sub>	60.080	1	60.080	0.30	0.69
5	Rock salt	0.0050	2.100	0.011	NaCl	102.957	1	102.957	0.51	0.54
	Organic part	0.2100	1.600	0.336						17.42
	Water	0.4000	1.000	0.400	H <sub>2</sub> O	18.000		18.000	7.20	20.74
	Total	1.000		1.929			20	1370.11	362.494	100.00

The molecular weight and density of the mineral constituents is enumerated below:

Inorganic components	Calcite	Hydroxylapatite	Magnesite	SiO <sub>2</sub>	Rock salt	Water
MW <sub>mineral</sub>	100.08	1004.67	84.32	60.08	102.957	18.00
$\rho_{\text{mineral}}$ (g/cm <sup>3</sup> )	2.70	3.10	3.00	2.65	2.10	1.00

The weight percentage composition of the mineral constituents in the inorganic component of bone tissue using mathematical modelling is presented in table 5. The table shows the composition of the oxides as determined by the ICP-OES technique, as well as the concentration values of the organic component, water and CO<sub>2</sub> determined by thermogravimetry.

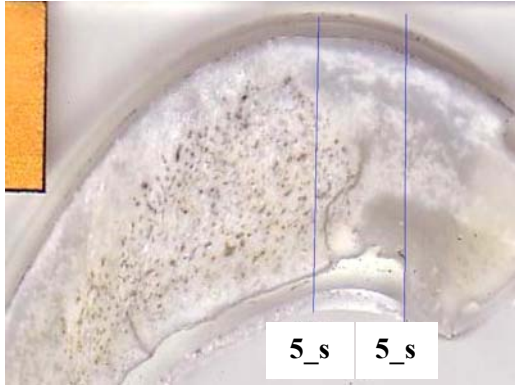
It may be concluded from the mathematical modelling of the weight percentage of the mineral constituents in the inorganic component of bone tissue and laboratory measurements done on the male bovine tibia that the properties of the bone tissue are primarily determined by its hydroxylapatite content. Since hydroxylapatite is constituted by CaO, P<sub>2</sub>O<sub>5</sub> oxides and bound water, the bone structure can be investigated by measurement of CaO distribution as can be determined with the LIPS technique.

In the present study, thin polished bone slides prepared from male bovine tibia were examined with laser induced plasma spectroscopy in a regular network and combined sampling system to derive the calculated calcium oxide concentration distribution. We particularly describe the relationship between irregularities experienced with regards to the bone structure and its CaO distribution.

The LIPS analyses of the thin polished bone slides were executed in a predetermined fashion as regards the region of interest (ROI) on the slides. The sampling strategy involved the consideration of the sampling system and sampling density. The ROI involved segmented and regular networks, and when both types of networks were employed to execute the analysis it was named as a combined sampling system. Thin polished bone slides Bull\_1, Bull\_2 and Bull\_5 were examined as enumerated above.

### LIPS analyses in segmented networks

Sample Bull\_5 was analyzed segmentally at 30 points (indicated in blue in figure below). The slide was 100  $\mu\text{m}$  thick and the 5<sup>th</sup> and the 6<sup>th</sup> segments were 13 mm and 15 mm in length, respectively. The sampling density of these two segments were 0.4 mm and 0.5 mm, respectively. The thin polished slide Bull\_5 with the 5<sup>th</sup> and the 6<sup>th</sup> segments(5\_sz 5 and 5\_sz 6) demarcated for LIPS analysis are shown below.



The emission spectrums of each ROI were analyzed using the LIPSBONE\_2013 software. The CaO concentration values were calculated using the CaO calibration curve.

Figures 3 and 4 (A and B) show the point by point CaO concentration values as per the segmental sampling approach. Figure 5A shows the 6<sup>th</sup> segment as it passes through the trabecular region of the bone tissue, and the resulting porotic CaO region typical for such region are well demarcated as represented by the trough in the corresponding curve.

#### LIPS analyses in regular networks

In this analytical approach, LIPS analyses of the thin polished tibia bone samples Bull\_1 and Bull\_2 was executed in square region of interests. Both trabecular and cortical regions were analyzed. The dimension of the squares was 4x4 mm. The total number of measurement points with the square amounted to a 100. These

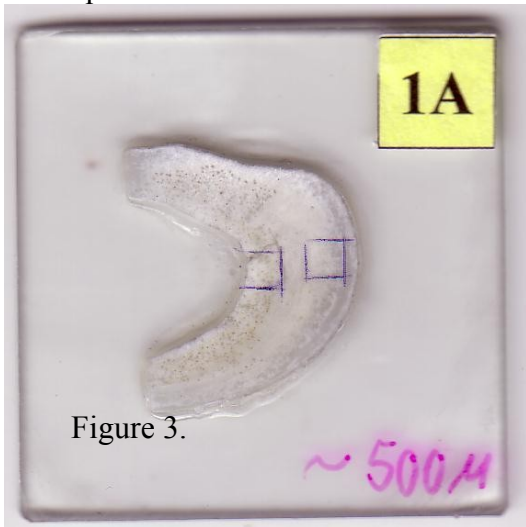


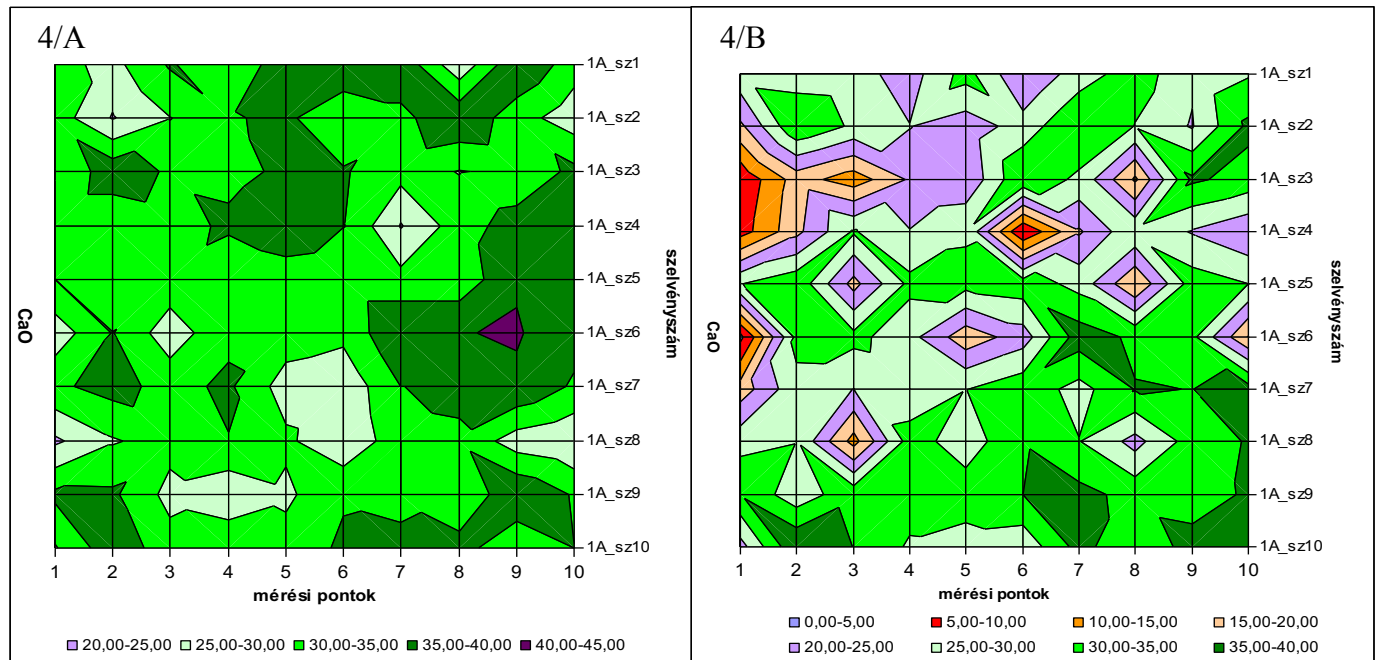
Figure 3.

100 points were placed over 10 segments, with a sampling density of 0.4 mm. The distance between the segments was 0.4 mm. Figure 3 illustrates the scanned picture of sample Bull\_1, where the square measurement regions are demarcated.

The CaO values as determined the LIPS analyses of square regions in the cortical part of sample Bull\_1 are presented in table 6. The average CaO concentration calculated in each segment was well within the standard of deviation, this implies to the relatively homogenous nature of the sample.

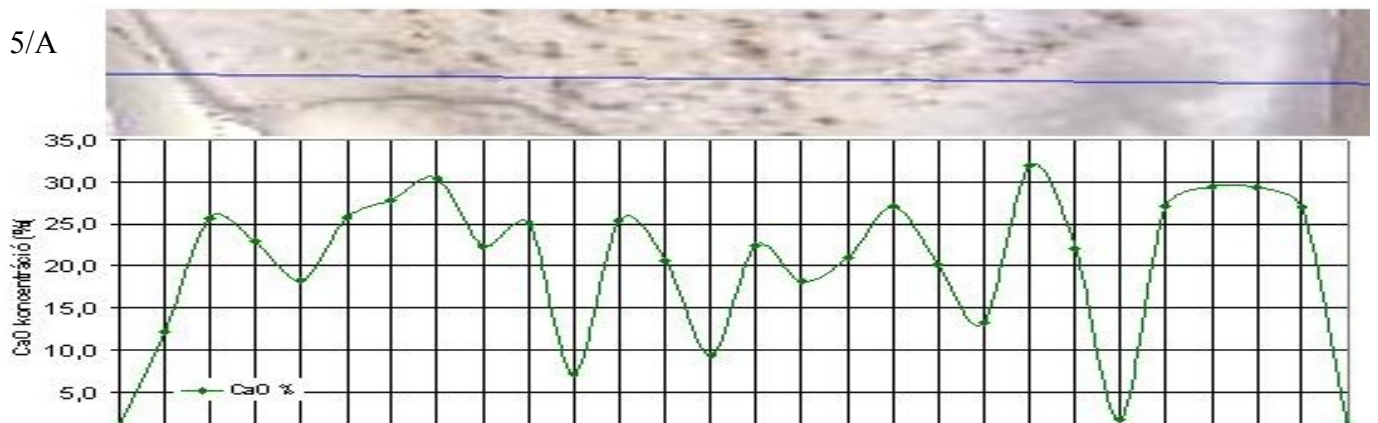
The homogeneity of the sample is illustrated in figure 4/A, where the superficial CaO distribution of the sample is depicted. Different CaO concentration ranges were detected in 3 regions, these are illustrated in different colours on the figure. The difference in the CaO elementary oxide concentrations was also underpinned by the calculated „frequency distribution” curves (figure 5/A), as such the

concentration values could be classified into three distinct groups.

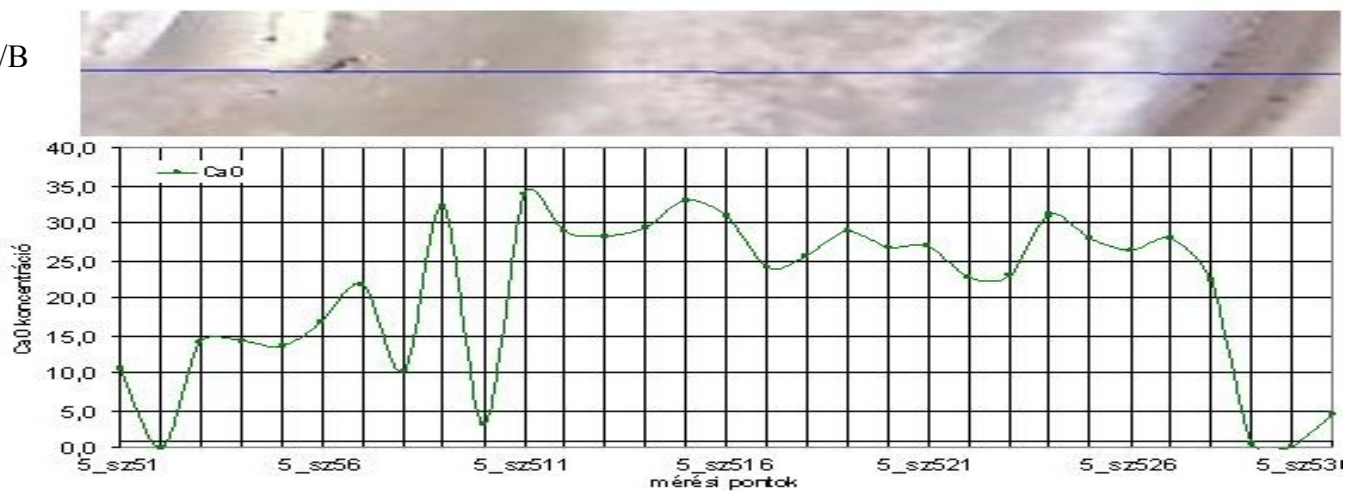


The average and coefficient of variation of the CaO concentration as determined by the LIPS analyses of square regions of interest in the trabecular part of sample Bull\_1 is summarized in table 5. The calculated average CaO concentration values in each segment, with the exception of segment number 1A-sz9 showed a larger variation as compared to the cortical findings, this leads us to the conclusion that the sample is of an inhomogenous structure.

5/A



5/B



The inhomogeneity of the sample is also depicted by the superficial CaO concentration distribution as illustrated in figure 4/B. The figure shows 6 regions of different CaO concentration ranges, these are shown in different colours.

The difference in the CaO elementary oxide concentrations was also underpinned by the calculated „frequency distribution” curves (figure 6/B), as such the concentration values could be classified into eight distinct groups (see below).

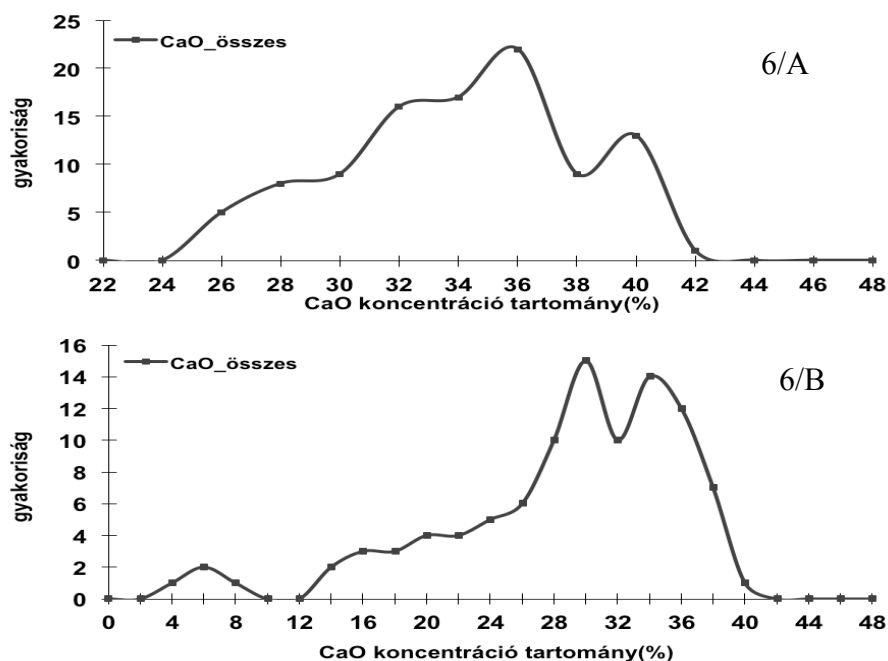
**Classification of CaO concentration values**

concentration ranges (%)	1. 0–5	2. 5–10	3. 10–15	4. 15–20	5. 20–25	6. 25–30	7. 30–35	8. 35–40
number	1	3	2	6	13	16	39	20

Table 5.

Segment	1	2	3	4	5	6	7	8	9	10	Average	CV
1A_sz1	28.41	27.44	26.88	22.90	31.98	20.08	27.43	32.67	25.97	29.45	27.32	3.80
1A_sz2	19.06	34.53	29.15	25.13	22.04	27.21	34.97	29.79	24.50	36.14	28.25	5.75
1A_sz3	5.71	17.41	12.10	20.60	21.03	34.46	28.81	14.15	35.83	33.13	22.32	10.35
1A_sz4	7.74	18.58	30.45	25.20	29.31	4.96	19.39	29.01	24.66	20.73	21.00	8.79
1A_sz5	29.85	33.66	18.17	31.36	31.78	32.93	28.30	15.27	32.44	30.06	28.38	6.38
1A_sz6	3.58	31.39	31.51	26.69	16.85	22.49	37.57	33.98	31.19	14.64	24.99	10.55
1A_sz7	17.43	28.55	24.98	26.31	29.89	33.29	28.14	35.25	34.94	37.44	29.62	5.95
1A_sz8	28.14	29.79	13.00	32.34	27.16	34.78	30.15	23.24	32.32	35.34	28.63	6.58
1A_sz9	34.64	26.88	33.40	32.53	32.93	35.00	36.49	33.39	32.21	35.81	33.33	2.67
1A_sz10	23.15	39.51	34.90	29.26	27.52	26.45	36.81	30.75	37.10	36.25	32.17	5.48
Average	19.77	28.77	25.45	27.23	27.05	27.17	30.81	27.75	31.12	30.90		
CV	11.00	6.82	8.28	4.05	5.38	9.48	5.69	7.65	4.58	7.59		

Figure 6.



Samples Bull\_1 and Bull\_2 were examined in a regular network framework and sample Bull\_5 was examined in a combined sampling system, overall a total of 460 points (regions) underwent LIPS analyses. The average CaO concentration values of the evaluated bone slides applying the LIPS technique are presented below:

Sample ID	all points	screened points	analysis	CaO concentration (%)	
				all	screened
Bull1A_trabecular_network	100	75	regular	27.60	31.55
Bull1A_cortical_network	100	100	regular	33.11	33.11
Bull2A_trabecular_network	80	44	regular	25.28	29.04
Bul2A_cortical_network	90	70	regular	29.22	30.68
Bull5_mixed_network	90	50	combined	24.77	28.89

CaO values below 25% were excluded from the final analysis. It may be concluded from our findings that the calculated CaO values were higher in the trabecular region as compared to the cortical one. In the table above, the „all points” represents all LIPS values attained in a squared fashion, and „screened” values represent those where the values of under 25% were excluded. As expected, the „screened” average CaO values were always higher than the „unscreened”.

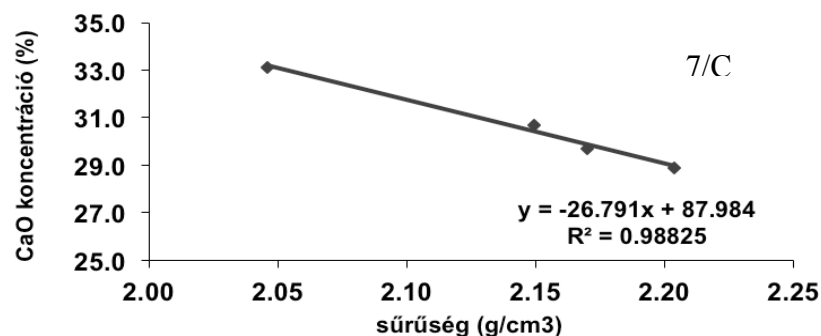
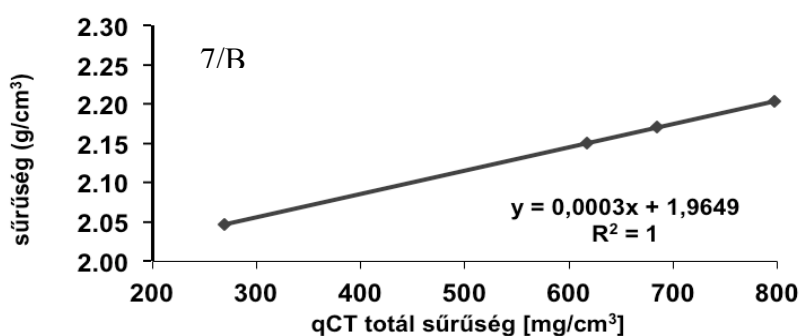
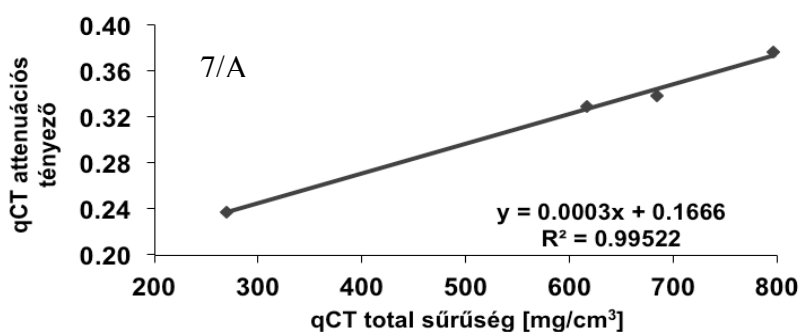
## Comparison of qCT measured attenuation coefficient with the geological density „ $\rho$ ” in male bovine tibia.

Male bovine bone samples prepared for the LIPS analyses were examined with qCT. The qCT results are presented below:

Male bovine tibia samples		Bull_1	Bull_2	Bull_3	Bull_4	Bull_5
qCT results	Total density (mg/cm <sup>3</sup> )	270.1	617.3	684.4	552.7	796.9
	Trabecular density (mg/cm <sup>3</sup> )	26.9	178.3	273.5	299.6	454.7
	Cortical density (mg/cm <sup>3</sup> )	469.0	976.3	1020.4	759.6	1076.8
	Attenuation coefficient	0.237	0.329	0.338	0.181	0.376

The attenuation coefficient as determined by qCT analysis is perhaps the best determinant of altered bone tissue structure. Primarily, we compared the qCT measured attenuation coefficient and total density, and there was significant correlation between the two.

Presuming that the qCT total density and the geological „ $\rho$ ” density are directly proportional, the qCT total density and the laboratory measured density (Bull\_2  $\rho = 2.150 \text{ g/cm}^3$ ) may be used to calculate the male bovine tibia „ $\rho$ ” density. The „ $\rho$ ” density and the qCT correlation is presented in figure 7/B. Furthermore, the correlation of „ $\rho$ ” density and the cortical average CaO concentration as measured by LIPS is presented in figure 7/C.



## MEDI-LIPS instrument: Summarized description

The MEDI-LIPS instrument has 4 main units: a measuring probe, a central processing unit, a fine positioning mechanical unit and „LIPS” software on a PC.

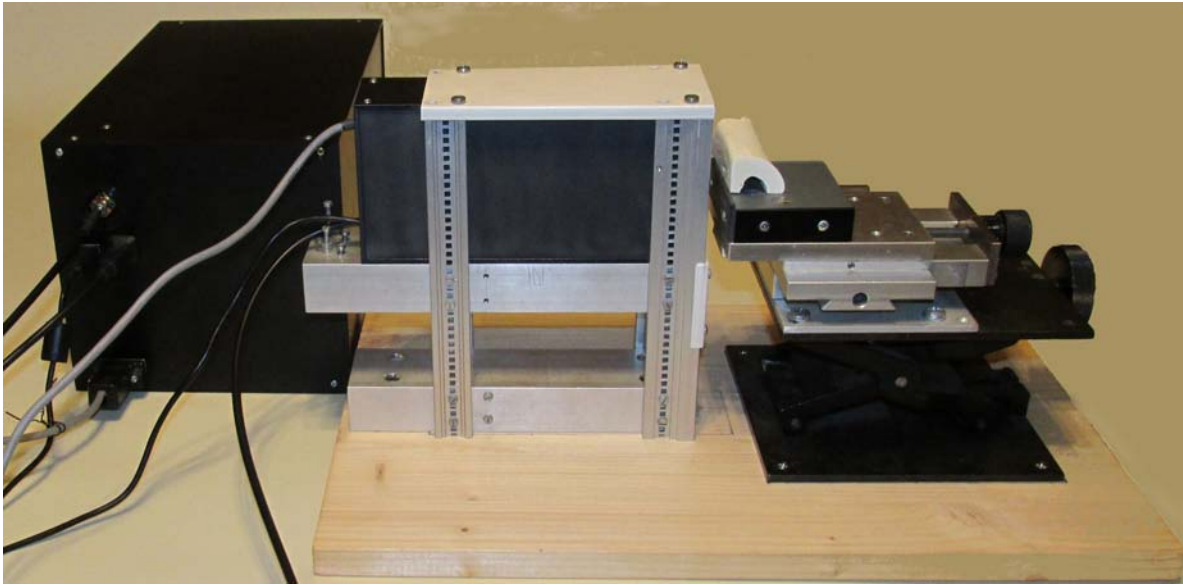


Figure 8. A picture of the MEDI-LIPS instrument with the laser head incorporated into the fine positioner.

The probe includes: - the Kigre Nd:YAG 1064 nm impulse laser with its trigger unit.

Also includes the laser beam expander and the laser focusing optics, additionally this also helps imaging the target area on the targeting camera's detector utilizing a beam splitter. The beam expander optic reduces the energy density of the laser beam, as not to damage the beam splitter's metallic dielectric coating. Additionally, the probe also couples the light of the generated plasma into the 1.5 meter quartz optical fiber. Furthermore, this unit also includes the white LED light used to illuminate the target surface.

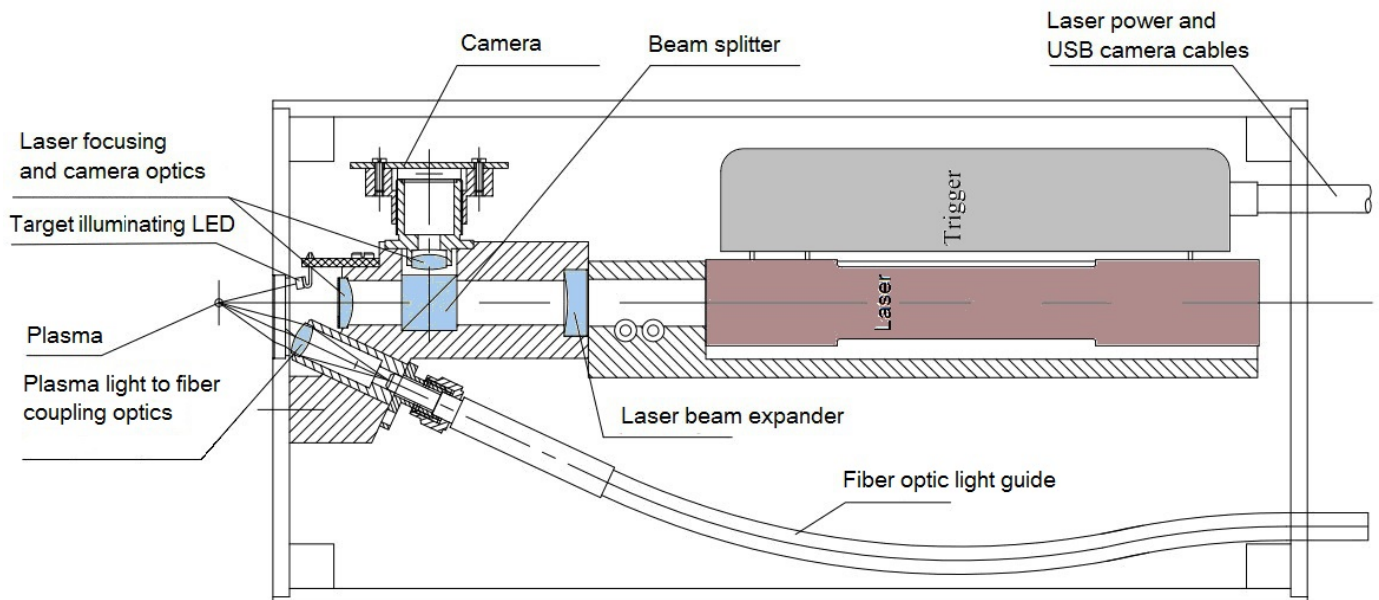


Figure 9. Cross-section of the laser head (probe)

The second main unit is the central processing unit. In this unit the most important part is the rotatable grating polychromator, dispersing the plasma light and focusing it onto the detector array's surface in the wavelength range between 200-800 nm, as such that only one 300 nm range is selectable in steps of 50 nm each.

As a result, one of the following wavelength ranges can be detected at a time:

200 - 500 nm  
250 - 550 nm  
300 - 600 nm  
350 - 650 nm  
400 - 700 nm  
450 - 750 nm  
500 - 800 nm

The rotation of the grating is achieved by a precision mechanics with stepper motor.

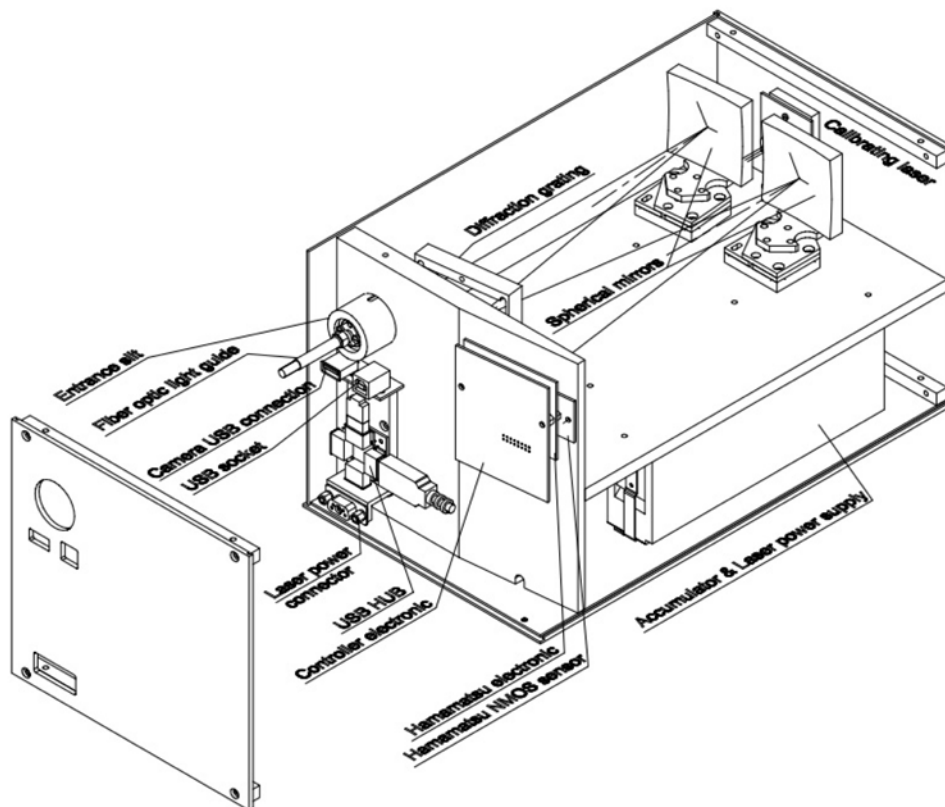


Figure 10. Axonometric projection of the central processing unit

The polychromator unit contains the quartz optic that collimates the plasma light, exiting the fibre optic, to polychromators entrance slit (dimensions of 50  $\mu\text{m}$  x 3 mm), 2 pcs. 50 x 50 mm spherical UV grade mirrors, 50 x 50 mm plain optical grating enabling the wavelength dependent resolution as demanded by the entrance slit, and 51.2 x 2.5 mm 2048 pixel HAMAMATSU diodes. Furthermore, it contains the 780 nm laser diode with aspheric optic used for crude wavelength calibration and a plain grating rotating stepper motor.

The central processing unit houses the processing electronics, the 1000V power supply of the Nd:YAG laser, the general power supply with various stabilized outputs and a 12 V 3 Ah gel Panasonic battery that can be charged externally. The processing electronics includes the HAMAMATSU low-noise, driver-amplifier electronic board and a microprocessor containing control board. The control panel's 16 bit analog-digital converter digitalizes the conditioned video signals and temporarily stores the recorded spectrums, furthermore it controls all internal subunits and connects via a USB and forwards all measured data to the computer for further assessment by the LIPS application run under a Windows operation system. The central processing unit also contains an USB HUB that allows connection of the probe's targeting camera and the processor to a computer via a single USB cable. The instrument does not include an on-off button, since it switches on automatically once the USB cable being connected to the computer.

## The „LIPS”processing software: instrument control and data analyzer program.

Constituent element (element oxides) analysis of elements known to constitute and verified by laboratory analysis were examined in animal and human bone samples. The LIPS program uses a standard element library composed of data from typical matrix and trace elements (toxic in most cases) as determined from reference samples in all 7 wavelength ranges. The standard element library contains those elements which may be of medical relevance and others that may find application in various research fields. Figures 11 and 12 present the LIPS standard element library in wavelength ranges of 200-500 nm and 500-800 nm, respectively.

H	STANDARD ELEMENTS																He
Li	Be											B	C	N	O	F	Ne
Na	Mg											Al	Si	P	S	Cl	Ar
K	Ca	Sc	Ti	V	Cr	Mn	Fe	Co	Ni	Cu	Zn	Ga	Ge	As	Se	Br	Kr
Rb	Sr	Y	Zr	Nb	Mo	Tc	Ru	Rh	Pd	Ag	Cd	In	Sn	Sb	Te	I	Xe
Cs	Ba	La	Hf	Ta	W	Re	Os	Ir	Pt	Au	Hg	Tl	Pb	Bi	Po	At	Rn
Fr	Ra	Ac															
Ce	Pr	Nd	Pm	Sm	Eu	Gd	Tb	Dy	Ho	Er	Tm	Yb	Lu				

Figure 11. The LIPS standard element library in the 200-500 nm wavelength range.

H	STANDARD ELEMENTS																He
Li	Be											B	C	N	O	F	Ne
Na	Mg											Al	Si	P	S	Cl	Ar
K	Ca	Sc	Ti	V	Cr	Mn	Fe	Co	Ni	Cu	Zn	Ga	Ge	As	Se	Br	Kr
Rb	Sr	Y	Zr	Nb	Mo	Tc	Ru	Rh	Pd	Ag	Cd	In	Sn	Sb	Te	I	Xe
Cs	Ba	La	Hf	Ta	W	Re	Os	Ir	Pt	Au	Hg	Tl	Pb	Bi	Po	At	Rn
Fr	Ra	Ac															
Ce	Pr	Nd	Pm	Sm	Eu	Gd	Tb	Dy	Ho	Er	Tm	Yb	Lu				

Figure 12. The LIPS standard element library in the 500-800 nm wavelength range.

The fractal reduction software that is used to reduce the thermic noise level is an integral part of the processing program. This software facilitates the use of mixed-normal (marked as IN in the program) amplitude (V1, V5) and mixed-integral-normal (VN1, VN5) amplitude values apart from allowing identification of elements and concentration calculation.

The MEDI-LIPS database system was set-up for each element of interest, where the spectral line wavelength value was selected from 5-10 spectral lines in the 200-800 nm wavelength range, in steps of 50 nm from each subsequent 300 nm region upon analysis of the high purity reference samples. These spectral lines are unequivocally identified by the software and assigned to the given element.

The rotatable grating may be positioned to detect one spectral range to another but this alone is insufficient for satisfactory evaluation. Furthermore, the built-in calibration laser only ensures the appropriateness of the selected wavelength range. The remaining, till a maximum of a few nanometers, spectral drift is corrected by the calibration module of the LIPS software. The correction is done by pre-defining the chief matrix element in advance, which in the case of bone samples is calcium.

The LIPS expert software was developed using the database system. The expert system primarily screens and short lists the database. It contains all maximum spectral line integral normal (IN), mixed-normal (V5) and mixed-integral-normal (VN5) amplitude values that the software detects during identification of an element. The new program module also utilizes these spectral lines for the calculation of the calibration equations and concentration values.

Table 6 presets the number of spectral lines in the standard element library (row 1), database system (row 2) and expert system (row 3) for matrix and trace elements as measured in the 200-500 nm wavelength range.

1	Al	Ba	Ca	Cu	Fe	Mg	Mn	Pb	Sí	Sr	Ti	Zn
2	4	5	5	9	17	5	10	4	5	4	15	4
3	1	1	1	1	1	1	1	1	1	1	1	1

Table 7 presets the number of spectral lines in the standard element library (row 1), database system (row 2) and expert system (row 3) for matrix and trace elements as measured in the 500-800 nm wavelength range.

1	Al	Ca	K	Li	Na	Sí
2	6	8	3	2	2	3
3	1	1	1	1	1	1

## Calibration of the MEDI-LIPS instrument

For calibration a total of 12 standard officially recognized samples from the Geological and Geophysical Institute of Hungary were used. Since trace elements such as Ba, Cu, Pb and Zn (toxic elements) are present in minute quantities in bone samples, barite and sulfide standard samples were also used.

Given the differences in the matrix properties of rocks, the available standard samples were classified into three groups (presented in table 8 through 10):

- Table 8: presents the element oxide composition of powdered rock mixed with WAX glue and pressed samples of schist, basalt, granite and limestone.
- Table 9: presents the element oxide composition of glass matrix samples (schist, basalt, granite and limestone) produced from powdered rock.
- Table 10: presents the composition of the barite and sulfide reference samples used for the calibration of Ba, Cu, Pb and Zn trace element concentration.

Table 8. Weight percentage composition of corrected element oxide concentration values of naturally occurring powdered rock mixed with WAX glue and pressed samples used for the calibration of the MEDI-LIPS instrument.

Calibrators	Sample ID	Al <sub>2</sub> O <sub>3</sub> [%]	CaO [%]	Fe <sub>2</sub> O <sub>3</sub> [%]	K <sub>2</sub> O [%]	MgO [%]	Na <sub>2</sub> O [%]	SiO <sub>2</sub> [%]	TiO <sub>2</sub> [%]
<b>Schist1/1</b>	Apaet11	17.17	0.275	5.750	3.225	1.617	1.10	50.16	0.000
<b>Basalt1/1</b>	Bazet11	13.50	5.39	8.083	0.167	6.225	3.87	41.25	0.950
<b>Granite1/1</b>	Gráet11	11.25	0.89	1.675	3.967	0.308	3.15	61.16	0.175
<b>Limestone1/1</b>	Méet11	2.00	39.83	0.767	0.341	0.617	0.00	7.16	0.108

Table 9. Weight percentage composition of corrected element oxide concentration values of naturally occurring powdered rock glass matrix samples used for the calibration of the MEDI-LIPS instrument.

Calibrators	Sample ID	Al <sub>2</sub> O <sub>3</sub>	CaO	Fe <sub>2</sub> O <sub>3</sub>	K <sub>2</sub> O	MgO	Na <sub>2</sub> O	SiO <sub>2</sub>	TiO <sub>2</sub>
		[%]	[%]	[%]	[%]	[%]	[%]	[%]	[%]
<b>Schist/4</b>	Apaet14	5.150	0.080	1.725	0.967	0.480	0.330	15.050	0.000
<b>Schist 1/6</b>	Apaet16	3.430	0.055	1.150	0.640	0.320	0.220	10.030	0.000
<b>Basalt1/4</b>	Bazet14	4.050	1.620	2.425	0.050	1.870	1.160	12.370	0.285
<b>Basalt1/6</b>	Bazet16	2.700	1.080	1.620	0.030	1.250	0.770	8.250	0.190
<b>Granite1/4</b>	Gráet14	3.370	0.267	0.502	1.190	0.092	0.940	18.350	0.052
<b>Granite1/6</b>	Gráet16	2.250	0.180	0.335	0.790	0.061	0.630	12.200	0.035
<b>Limestone1/4</b>	Méset14	0.600	11.950	0.230	0.102	0.180	0.000	2.150	0.032
<b>Limestone1/6</b>	Méset16	0.400	7.966	0.150	0.068	0.120	0.000	1.430	0.020

Table 10. The composition of the barite and sulfide reference samples used for the calibration of Ba, Cu, Pb and Zn trace element concentrations.

Pastille ID	Sulphide ore	Quartz sand	Pb	Zn	Cu
	gram	gram	ppm	ppm	ppm
<b>1</b> <b>2</b> <b>3</b> <b>4</b> <b>5</b> <b>6 (undiluted)</b>  <b>8</b> <b>9</b> <b>10</b> BaSO <sub>4</sub> Mol. weight Ba content	0	200	0	0	0
	2	198	388	464	45
	5	195	970	1160	113
	10	190	1940	2320	225
	20	180	3880	4640	450
	50	150	9700	11600	1125
	200	0	38800	46400	4500
	<b>BaSO<sub>4</sub></b>	<b>Quartz sand</b>	<b>Ba</b>		
	gram	gram	ppm		
	1	199	2943		
	2	198	5886		
	4	196	11771		
	233.33 0.588565551				
<b>Diluted</b>	<b>10x</b>	<b>Quartz sand</b>	<b>Ba</b>		
<b>6</b> <b>7</b>	gram	gram	ppm		
	10	190	589		
	20	180	1177		

For reliable calculation of the inorganic element oxide concentration values in bone samples, an independent calibration equation was produced for each element oxide. For calibration a minimum of three, but as many as possible, spectrum are desired from reference samples of various concentrations. The calibration equations – as per the element emission spectrum of the studied reference samples – can be calculated based on the strongest interference-free spectral lines peak amplitude values. The peak values may be integral-normal, mixed-normal (V1, V5) or mixed-integral-normal (V1N, V5N) amplitudes.

5 different types of regression equations were used:

Power equation (Malpica)	$I = P_3 * c^{P_2 * c}$
Exponential equation	$I = P_3 * \exp(P_2 * c)$
Logarithmic equation	$I = P_1 * \log(c) + P_0$
Linear equation	$I = P_1 * c + P_0$
Second degree polynomial equation	$I = P_3 * c^2 + P_2 * c + P_0$

where:

I	peak amplitude of the spectral line, second derived, mixed-normal (1) and mixed-normal (5) amplitude value
$P_0, P_1, P_2$ and $P_3$	parameter vectors to be determined by calibration
c	concentration value of the element oxide

Table 11 summarizes  $P_0, P_1, P_2$  és  $P_3$  parameter vectors, the square of the correlation coefficient, the type of normalization and equation, and the upper and lower values of the concentration values in the equations for the respective matrix and trace elements.

	wavelength	parameter vectors, correlation coefficients								
	$\lambda$	P <sub>3</sub>	P <sub>2</sub>	P <sub>1</sub>	P <sub>0</sub>	R <sup>2</sup>				
Al <sub>2</sub> O <sub>3</sub>	309.350	917.54	1.3499	-16.106	0.7277	0.9901	V5	Po	0.0	20.0
CaO	393.050		151.1900			1.0000	VN	Pl	0.0	60.0
Fe <sub>2</sub> O <sub>3</sub>	275.050	0.4863	131.2800			0.9978	V5	Ex	0.0	10.0
K <sub>2</sub> O	766.642	47921.0000	2.5755			0.9836	V5	Po	0.0	40.0
MgO	279.850	375.8100	2.1997			0.9999	V5	Po	0.0	10.0
Na <sub>2</sub> O	589.026	3404.4000	2.6321			1.0000	V5	Po	0.0	4.0
SiO <sub>2</sub>	252.057	43813.0000	1.4843	29.295	159.2400	0.9816	V5	Po	0.0	7.0
SiO <sub>2</sub>	252.057					0.9890	V5N	Ln	7.0	100.0
TiO <sub>2</sub>	323.619	0.0637	126.4000			0.9999	V5	Ex	0.0	3.0

Table 12 summarizes  $P_0, P_1, P_2$  és  $P_3$  parameter vectors, the square of the correlation coefficient, the type of normalization and equation, and the upper and lower values of the concentration values in the equations for the trace elements.

	wavelength	parameter vektors, correlation coefficients								
	$\lambda$	P <sub>3</sub>	P <sub>2</sub>	P <sub>1</sub>	P <sub>0</sub>	R <sup>2</sup>				
Ba_I	455.464			9.602	-0.0054	0.9995	V5	Ln	0.0	1.0
Cu_I	324.935	1024	1.8443			0.9995	V5	Po	0.0	1.0
Mn_I	403.150	0.0002	3342.3			0.9889	V5	Ex	0.0	1.5
Pb_I	405.735			58.555	-0.1187	0.9908	V5	Ln	0.0	2.0
Sr_II	407.666	43.9780	1.6674			0.9976	V5	Po	0.0	1.0
Zn_I	334.357	-287169	11633	-64.903	0.0977	1.0000	V5	Po	0.0	2.0

An independent calibration equation was proposed for reliable calculation of concentration values for each element (element oxide) examined in the bone samples. The calibration equation parameter vectors were determined based on the strongest interference-free spectral lines mixed-normal (V5) and mixed-integral-normal (V5N) peak amplitude values. The strongest spectrum lines wavelength values are presented in table 6.

For evaluation of the measured spectrums in the 200-500 nm and 500-800 nm wavelength ranges the *MEDI\_LIPS\_2048\_200* and *MEDI\_LIPS\_2048\_500* calibration files were created.

Figure 13 and 14 present the laser induced plasma spectrum of a powdered rock WAX glue mixed basalt pressed sample and its „web camera” picture in the wavelength ranges of 200-500 nm and 500-800 nm. The element oxide composition of the sample is presented in zoom in figure 8.

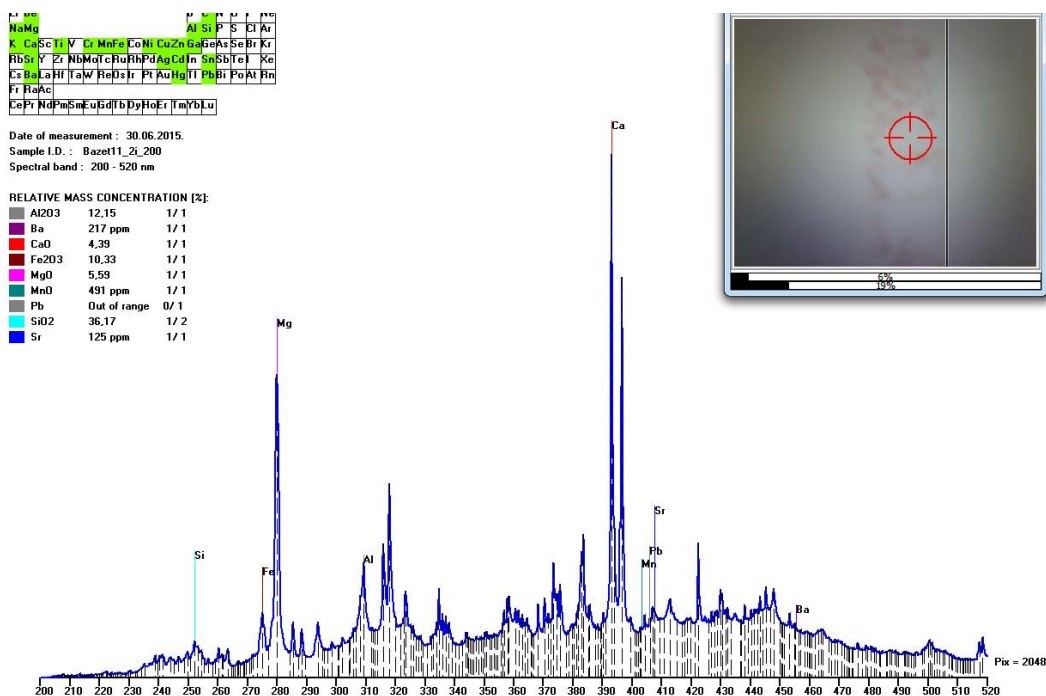


Figure 13. Powdered rock and WAX glue mixed basalt (Bazet11\_2i\_200) pressed sample laser induced plasma spectrum in the 200-500 nm wavelength range and its web camera picture with an electronic targeting cross.

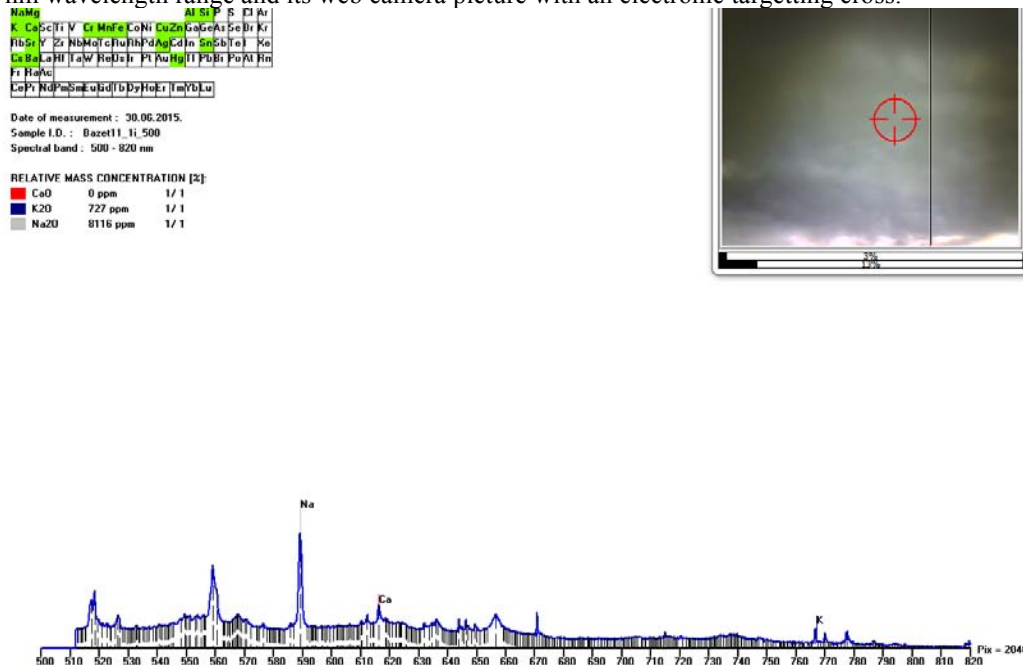


Figure 14. Powdered rock and WAX glue mixed basalt (Bazet11\_li\_200) pressed sample laser induced plasma spectrum in the 500-800 nm wavelength range and its web camera picture with an electronic targeting cross.

The element oxide composition in the 200-500 nm wavelength range of the sample in zoom is presented in figure 15.










RELATIVE MASS CONCENTRATION [%]:		
	Al <sub>2</sub> O <sub>3</sub>	12,15 1/ 1
	Ba	217 ppm 1/ 1
	CaO	4,39 1/ 1
	Fe <sub>2</sub> O <sub>3</sub>	10,33 1/ 1
	MgO	5,59 1/ 1
	MnO	491 ppm 1/ 1
	Pb	Out of range 0/ 1
	SiO <sub>2</sub>	36,17 1/ 2
	Sr	125 ppm 1/ 1

Figure 15. Basalt (Bazet11\_2i\_200) reference sample element oxide composition and the calculated concentration values.

The individual elements (element oxides) are demarcated with different colours in figure 15. The concentration values are presented in percentage (%) and parts per million (ppm). Besides the concentration values the identified and all spectral lines number are presented as derived by the expert software analysis.

## Conclusions

1. With the applied pre-analytical treatments and analytical procedures the total composition of the studied bone samples was definable.
2. The inorganic/mineral composition of the examined bones is (carbonate)-apatite, carbonates and salts (~65 wt.%), whereas the organic part is composed of collagens (~35 wt.%).
3. For the exact definition of the apatite and the salts it would be necessary to carry out Cl and F analysis preferentially using electron microprobe analysis (EMPA).
4. From a medical point of view the composition of the studied bones (apart from As-and due to suspicion of contamination –Fe, Al, Ni, Sn and Pb) could be reliably examined.
5. There was a significant inverse correlation between the bone density and age in the examined female human bone samples. Although this was not entirely true for the male samples, it was found that the bone density showed inverse correlation mainly in those samples that belonged to the most elderly.
6. It was interesting to note that the DTA measured adsorption water content reduced with increasing age of the bone samples studied. The absorption water content is usually dependent on particle size or the inconsistency in the charge of the minerals in the sample. This may suggest that the average particle size increases and the charge of the minerals becomes more consistent with age. Although the method of sample preparation needs also to be taken into consideration, this should not be a measure of the age of the bone sample.
7. In the female samples, it was noted that with increase in age there was increase in CO<sub>3</sub> → PO<sub>4</sub> displacement (as determined by the area under the curve for CO<sub>3</sub> and CO<sub>3</sub>/(CO<sub>3</sub>+PO<sub>4</sub>)) as per the infra findings, however, this was not the case in the male samples.
8. Although only a tendency, in the case of the female samples, CO<sub>3</sub> → PO<sub>4</sub> displacement was inversely correlated to the total bone density of the samples.
9. The infra results showed that increase in CO<sub>3</sub> → PO<sub>4</sub> displacement went hand in hand with the increase in the molecular water content presumably with binding to the hydroxyl apatite structure.
10. It seems that the normalized CaO content does not show a correlation with age, in other words, we observed no increase or otherwise with increasing age in this elements' measured concentration.
11. Interestingly, it seems that the amount of cobalt in the sample is catalyzing the CO<sub>3</sub> → PO<sub>4</sub> displacement in the studied bone samples.

## Alterations from the original research plan

The following two points were also part of the original research plan:

1. To develop a new instrument suitable for in vivo human assessments and to develop a protocol that is not painful and ethically acceptable.
2. To assess other applications in medicine, such as drug accumulation and toxicology.

The above two were not feasible in the time and financial support requested and granted for the present research project.

## Finance and publications

The research fund was basically used as specified in the research plan, but some funds were reallocated primarily to finance the development of the MEDI-LIPS instrument. A very small part of the research fund allocated for the first year was used to finance the completion of previous research. The following articles, with this regard, have been accepted for publication, where the funding from the present research grant is duly acknowledged:

J Bone Miner Metab. 2013 [Epub] DOI 10.1007/s00774-013-0451-z

Immunol Res 2013 [Epub] DOI 10.1007/s12026-013-8405-z

Immunol Res 2013 [Epub] DOI 10.1007/s12026-013-8425-8

Clin Rheumatol. 2013 Aug;32(8):1161-7.

PLoS One. 2014 Mar 12;9(3):e91647. doi: 10.1371/journal.pone.0091647. eCollection 2014.

Clin Chem Lab Med. 2014 May 15. pii: /j/cclm.ahead-of-print/cclm-2014-0041/cclm-2014-0041.xml. doi: 10.1515/cclm-2014-0041.

Lege Artis Medicinae. Kalcium Interdiszciplináris Fórum (LAM KID) 2014;4(2):63–68.

Lege Artis Medicinae. Kalcium Interdiszciplináris Fórum (LAM KID) 2014;4(4):155–161.

Osteoporosis Int 2015; 26:1965–1970 DOI 10.1007/s00198-015-3069-2

BMC Musculoskeletal Disorders 2015 Aug 28;16(1):227. doi: 10.1186/s12891-015-0684-1.

Articles related directly to the present research:

Andrássy L, Maros G, Kovács IJ, Horváth Á, Gulyás K, Bertalan É, Besnyi A, Fűri J, Fancsik T, Szekanecz Z, Bhattoa HP. Lézer-alapú geológiai technikák felhasználhatósága a csontkutatásban: kalcium oxid eloszlás vizsgálatok állati csont vékonycsiszolatokon. Orvosi Hetilap 2014;155(45):1783-93. doi: 10.1556/OH.2014.30010.

Kovács I, Udvardi B, Falus G, Földvári M, Fancsik T, Kónya P, Bodor E, Mihály J, Németh C, Czirják G, Ősi A, Vargáné Barna Z, Bhattoa HP, Szekanecz Z, Turza S. Az ATR FTIR spektrometria gyakorlati alkalmazása néhány - elsősorban földtani - esettanulmány bemutatásával. Földtani Közlöny 2015;145(4):173-192.

## References

1. Ralston SH. *Best Pract Res Clin Rheumatol* 2005;19(3):487-501.
2. Griffith JF, Genant HK. *Best Pract Res Clin Endocrinol Metab* 2008;22(5):737-64.
3. Garcia F, Ortega A, Domingo JL, Corbella J. *J Environ Sci Health A Tox Hazard Subst Environ Eng* 2001;36(9):1767-86.
4. Uryu T, Yoshinaga J, Yanagisawa Y, Endo M, Takahashi J. *Anal Sci* 2003;19(10):1413-6.
5. Seltzer MD, Lance VA, Elsey RM. *Sci Total Environ* 2006;363(1-3):245-52.
6. Hetter KM, Bellis DJ, Geraghty C, Todd AC, Parsons PJ. *Anal Bioanal Chem* 2008;391(6):2011-21.
7. Schutz A, Olsson M, Jensen A et al. *Int Arch Occup Environ Health* 2005;78(1):35-43.
8. Raffalt AC, Andersen JE, Christgau S. *Anal Bioanal Chem* 2008;391(6):2199-207.
9. Shafer MM, Siker M, Overdier JT, Ramsel PC, Teschler-Nicola M, Farrell PM. *Sci Total Environ* 2008;401(1-3):144-61.
10. Li R, Yang H, Wang K. *Beijing Da Xue Xue Bao* 2003;35(6):622-4.
11. Malluche HH. *Nephrol Dial Transplant* 2002;17 Suppl 2:21-4.
12. Bervoets AR, Oste L, Behets GJ, Dams G, Blust R, Marynissen R, et al. *Bone* 2006;38(6):803-10.
13. Wang X, Yuan L, Huang J, Zhang TL, Wang K. *J Cell Biochem* 2008;105(5):1307-15.
14. Kazantzis G. *Biomaterials* 2004;17(5):493-8.
15. Pitt MA. *Agents Actions* 1976;6(6):758-69.
16. Shih RA, Hu H, Weisskopf MG, Schwartz BS. *Environ Health Perspect* 2007;115(3):483-92.
17. Carmouche JJ, Puzas JE, Zhang X et al. *Environ Health Perspect* 2005;113(6):749-55.
18. Lowe NM, Fraser WD, Jackson MJ. *Proc Nutr Soc* 2002;61(2):181-5.
19. Palacios C. *Crit Rev Food Sci Nutr* 2006;46(8):621-8.
20. Mak TW, Shek CC, Chow CC, Wing YK, Lee S. *J Clin Endocrinol Metab* 1998;83(11):3857-9.
21. Tannirandom P, Epstein S. *Osteoporos Int* 2000;11(8):637-59.
22. Kitchin B, Morgan SL. *Curr Rheumatol Rep* 2007;9(1):85-92.
23. Aslam, Chettle DR, Pejovic-Milic A, Waker AJ. *Phys Med Biol* 2009;54(1):17-28.
24. Weinberg ED. *Pediatr Endocrinol Rev* 2008;6(1):81-5.
25. Reginster JY. *Rev Med Liege* 2007;62(11):685-7.
26. Burlet N, Reginster JY. *Clin Orthop Relat Res* 2006;443:55-60.
27. Radziemski LJ. *Microchem J* 1994;50(3):218-234.
28. Phipps C, Luke J, Funk D, Moore D, Glowina J, Lippert T. *Appl Surf Sci* 2006;252(13):4838-4844.
29. Salle B, Cremers DA, Maurice S, Wiens RC. *Spectrochim Acta B* 2005;60:805-815.
30. Harmon RS, Lucia FC, Miziolek AW, McNesby KL, Walters RA, French PD. *Geochem-Explor Environ Anal* 2005;5(1):21-28.
31. Bolger JA. *Appl Spectrosc* 2000;54(2):181-189.
32. Maros G, Palotas K. Conference Proceeding - Fluids and Fractures in the Lithosphere, 26-27th March, 1999, Nancy, France, 1999. p. 92.
33. Maros G, Pasztor S. *European Geologist* 2001;12:40-43.
34. Maros G, Palotas K. *MAFI jelentese 1999-ról*. Budapest, Hungary;2000. p. 315-339.
35. Maros G, Palotas K, Koroknai B, Sallay E. *Bull Geosci* 2002;77(2):105-112.
36. Maros G, Koroknai B, Palotas K et al. *MAFI jelentese 2003-ról*. Budapest, Hungary;2004. p. 371-394.
37. Maros G. PhD dissertation, University of Miskolc, Hungary;2006.
38. Maros G, Andrassy L, Zilahi-Sebess L, Mathe Z. *First Break* 2008;26(6):143-152.
39. Andrassy L, Maros G, Sallay E. Conference proceeding-Joint meeting of MFT, MGE, OMBKE and SPE - Geotechnical challenges at the turn of the century- Szolnok, Hungary, 2000. p. 5.
40. Andrassy L, Zilahi-Sebes L, Vihar L. *Geophys Transac* 2003;44(1):95-138.
41. Maros G, Andrassy L, Mara J, Vihar L, Zilahi-Sebes L. Conference proceeding-Meeting of the International Conference on Geophysics, Geology, Fluid mining and Environment protection, Szolnok, Hungary, 2003, A16.
42. Földessy J, Maros G, Andrassy L, Kaposvari F, Dezső J. 8th International conference on acid rock drainage (ICARD), Skelleftea, Sweden, June 22-26 2009. <http://www.proceedings-stfandicard-2009.com/>
43. Andrassy L, Maros G. *Hung Geophys* 2011;52(2):62-78.
44. Gomez I, Szabo A, Pap L Jr, Pap L, Boda K, Szekanecz Z. *Phys Ther* 2012;92(2):289-97.
45. Pap L, Gomez I, Pap L Jr, Szabo A, Szekanecz Z. *Joint Bone Spine* 2010;77(5):426-31.
46. Rass P, Pakozdi A, Lakatos P et al. *Rheumatol Int* 2006;26(11):964-71.
47. Bodolay E, Bettembuk P, Balogh A, Szekanecz Z. *Clin Rheumatol* 2003;22(3):213-7.
48. Bhattoa HP, Bettembuk P, Ganacharya S, Balogh A. *Osteoporos Int* 2004;15(6):447-51.
49. Bhattoa HP, Bettembuk P, Balogh A, Szegedi G, Kiss E. *Osteoporos Int* 2004;15(5):396-404.
50. Bhattoa HP, Bettembuk P, Balogh A, Szegedi G, Kiss E. *Clin Rheumatol* 2002;21(2):135-41.
51. Bhattoa HP, Kiss E, Bettembuk P, Balogh A. *Rheumatol Int* 2001;21(3):97-102.
52. Wang X, Zuo Y, Huang D, Hou X, Bao Y. *Biomed Environ Sci* 2010;23:473-480.
53. Alvarez-Lloret P, Rodríguez-Navarro AB, Romanek CS, Gaines KF, Congdon JMACLA 2006;6:45-47.
54. Foldvari M. Occasional Papers of the Geological Institute of Hungary 2011;213:1-180.
55. Toth J, Udvardi B, Kovacs IJ et al. *MOL Scientific Magazine* 2012;1:52-61.
56. Pleshko N, Boskey A, Mendelsohn R. *Biophys J* 1999;60:786-793.
57. Stathopoulou ET, Psycharis V, Chrysikos GD, Gionis V, Theodorou G. Bone diagenesis: *Palaeogeogr Palaeoclimatol Palaeoecol* 2008;266:168-174.
58. Paschalis EP. *Osteoporos Int* 2009;20:1043-1047.
59. Pasteris JD, Yoder CH, Wopenka B. *Am Mineral* 2014;99:16-27.